Inorganic Chemistry

Article

pubs.acs.org/IC

A New UV Nonlinear Optical Material $CsZn_2B_3O_7$: ZnO_4 Tetrahedra Double the Efficiency of Second-Harmonic Generation

Sangen Zhao,[†] Jia Zhang,[‡,§] Shu-quan Zhang,[†] Zhihua Sun,[†] Zheshuai Lin,*[,‡] Yicheng Wu,[‡] Maochun Hong,[⊥] and Junhua Luo*[,†]

[†]Key Laboratory of Optoelectronic Materials Chemistry and Physics, Fujian Institute of Research on the Structure of Matter, Chinese Academy of Sciences, Fuzhou, Fujian 350002, China

[‡]Beijing Center for Crystal R&D, Key Lab of Functional Crystals and Laser Technology of Chinese Academy of Sciences, Technical Institute of Physics and Chemistry, Chinese Academy of Sciences, Beijing 100190, China

[§]University of Chinese Academy of Sciences, Beijing 100049, China

[⊥]State Key Laboratory of Structural Chemistry, Fujian Institute of Research on the Structure of Matter, Chinese Academy of Sciences, Fuzhou, Fujian 350002, China

Supporting Information

ABSTRACT: A new noncentrosymmetric borate $CsZn_2B_3O_7$ was synthesized by the solid-state reaction techniques. The crystals were obtained by flux method and are of block shape without layering tendency. Single-crystal X-ray diffraction analysis reveals that the crystal structure is composed of $[Zn_2BO_5]_\infty$ two-dimensional layers that are bridged by $[B_3O_6]^{3-}$ groups to form a three-dimensional framework with one-dimensional channels occupied by Cs^+ cations along the *a* and *c* axes. Thermal analysis indicates that $CsZn_2B_3O_7$ melts incongruently. UV−visible−near-IR diffuse reflectance spectrum gives a short absorption edge at 218 nm. $CsZn_2B_3O_7$ is phase-matchable, with a powder second-harmonic generation (SHG) efficiency of 1.5 × KDP (KDP, potassium dihydrogen phosphate) at 1064 nm, based on the Kurtz−Perry method. These results show that $CsZn_2B_3O_7$ may have prospects as a UV nonlinear optical material. Interestingly, the SHG efficiency of $CsZn_2B_3O_7$ is about twice that of γ-$KBe_2B_3O_7$, a structurally analogous alkaline and alkaline earth borate. First-principles calculations combined with atom-cutting analysis reveal that the ZnO_4 tetrhedral groups in $CsZn_2B_3O_7$ account for the SHG enhancement.

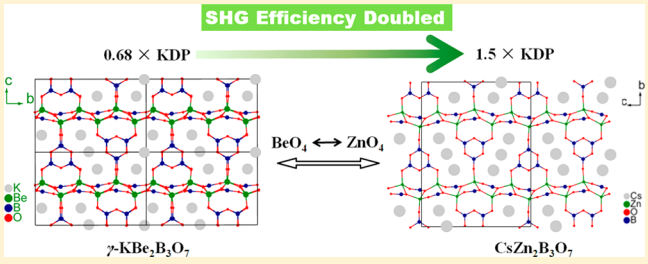

1. INTRODUCTION

UV nonlinear optical (NLO) materials are of current interest and great importance in laser science and technology, as they can expand the wavelength range of common laser sources to the UV spectral region.[1] The prerequisite of a NLO material is that it should be crystallographically noncentrosymmetric (NCS), and the common strategy to predesign NCS structures is to employ asymmetric structural units as fundamental building blocks,[2] such as second-order Jahn−Teller (SOJT) distorted octahedra of d^0 cation centers (Ti^{4+}, V^{5+}, Mo^{6+}, etc.),[3] stereoactive lone pair cations (Bi^{3+}, Te^{4+}, I^{5+}, etc.),[4] polar chalcogenide units ($[AsS_3]^{3-}$, $[SbS_3]^{3-}$, $[TeS_3]^{2-}$, etc.),[5] or borate π-orbital systems.[6] For UV NLO applications, however, the additional requirements should be imposed on the optical properties of the desired materials; that is, wide transparency window down to UV region, large second-harmonic generation (SHG) coefficients, and sufficient birefringence to achieve the phase-matching condition. In a material, the presence of large SHG coefficients is, to some extent, in contradiction to the wide UV-transparent window.[7] For instance, the SOJT octahedra, stereoactive lone pair cations, as well as polar chalcogenide units, can produce a large SHG response when they are arranged in a "constructive" manner alone or combined,[8] for example, in $BaTeM_2O_9$ (M = Mo, W),[8e−g] $TiO(IO_3)_2$,[8h] and $A_3Ta_2AsS_{11}$ (A = K, Rb);[8i] nevertheless, they can also cause the UV absorption edge of a material to evidently red shift, and thus the resultant materials are usually not transparent in UV region. In comparison, borate π-orbital systems are not only NLO-active but also UV-transparent. Moreover, their planar configurations can give rise to large optical anisotropy, that is, birefringence. Therefore, borate systems are especially suitable for UV NLO applications.

Over the past decades, the intensive studies on borate systems have led to the discovery of many UV NLO materials, such as LiB_3O_5 (LBO),[9] β-BaB_2O_4 (BBO),[10] $CsLiB_6O_{10}$ (CLBO),[11] and $KBe_2BO_3F_2$ (KBBF).[12] In particular, KBBF is attracting more and more attention because of its unique and crucial role in a number of advanced scientific instruments using deep-UV laser sources.[13] In the structure of KBBF, the

Received: October 23, 2013
Published: February 10, 2014

   dx.doi.org/10.1021/ic402667m | Inorg. Chem. 2014, 53, 2521−2527

NLO-active $[BO_3]^{3-}$ groups in the $[Be_2BO_3F_2]_\infty$ layers are coplanar and aligned, giving rise to a relatively large SHG response and a sufficient birefringence. Unfortunately, KBBF suffers a strong layering tendency that originates from the weak K^+-F^- ionic interactions between the adjacent $[Be_2BO_3F_2]_\infty$ layers. This has led to a great difficulty in the growth of thick KBBF crystals.[13] To mitigate the layering tendency while preserving the desired optical properties for NLO applications, chemists have discovered or designed a number of borates with layered structural units connected by anionic groups.[14] Recently, Ye and co-workers[14d] discovered a series of NCS alkaline beryllium borates, including β-$KBe_2B_3O_7$, γ-$KBe_2B_3O_7$, and $RbBe_2B_3O_7$, which consist of $[Be_2BO_5]_\infty$ layers connected by $[BO_2]_\infty$ chains or $[B_3O_6]^{3-}$ planar groups. For these NCS borates, the covalent bonds between the $[Be_2BO_5]_\infty$ layers provide strong interlayer connections that would be helpful to eliminate the layering tendency, but their SHG efficiencies are relatively small (<potassium dihydrogen orthophosphate (KDP)), owing to the long distances between the $[Be_2BO_5]_\infty$ layers. In this Paper, we report a new NCS borate $CsZn_2B_3O_7$ whose structure is analogous to that of γ-$KBe_2B_3O_7$. Interestingly, $CsZn_2B_3O_7$ exhibits a SHG efficiency of about 2-fold that of γ-$KBe_2B_3O_7$. The first-principles calculations and atom-cutting analysis indicate that the SHG enhancement mainly originates from the ZnO_4 tedrahedra. This Work distinguishes ZnO_4 tedrahedra as a new type of UV-transparent NLO-active units. We will also report the synthesis, crystal growth, structure, and thermal behavior as well as the linear and nonlinear optical properties of $CsZn_2B_3O_7$ in this Paper.

2. EXPERIMENTAL METHODS

Reagents. Cs_2CO_3 (Aladdin, 99%), ZnO (Sinopharm, 99.0%), ZnF_2 (Sinopharm, 95.0%), and H_3BO_3 (Sinopharm, 99.5%) were used as received.

Synthesis of $CsZn_2B_3O_7$. Polycrystalline samples of $CsZn_2B_3O_7$ were synthesized by the traditional solid-state reaction techniques. A mixture of Cs_2CO_3 (0.326 g, 0.001 mol), ZnO (0.326 g, 0.004 mol), and H_3BO_3 (0.371 g, 0.006 mol) was thoroughly ground, heated to 500 °C at a rate of 50 °C/h, and then sintered at this temperature for 24 h. The products were cooled to room temperature, ground thoroughly, and then sintered at 800 °C for 120 h with no less than one intermediate grinding. Polycrystalline $CsZn_2B_3O_7$ powders were obtained, and the phase purity was confirmed by powder X-ray diffraction (XRD) analysis, which was carried out at room temperature on a Rigaku MiniFlex II diffractometer equipped with Cu Kα radiation. The scanning step width of 0.02° and scanning rate of 0.05° s^{-1} were applied to record the patterns in the 2θ range of 10−70°. The measured powder XRD pattern matches the one calculated from single-crystal XRD analysis very well (see Figure S1 in the Supporting Information).

Crystal Growth. Single crystals of $CsZn_2B_3O_7$ were grown with a $Cs_2O-ZnF_2-B_2O_3$ flux system by a spontaneous nucleation approach. A mixture of Cs_2CO_3 (4.88 g, 0.015 mol), ZnO (0.81 g, 0.01 mol), ZnF_2 (2.07 g, 0.02 mol), and H_3BO_3 (2.47 g, 0.04 mol) was thoroughly ground and placed into a platinum crucible. The crucible was rapidly heated to 700 °C in a temperature-programmable electric furnace and then held at this temperature for 2 d. Another 2.47 g H_3BO_3 (0.04 mol) was added to the mixture after the crucible was cooled to room temperature. The temperature was subsequently increased to 1000 °C and then held for 1 d to ensure that the melt was homogenized. The melt was cooled slowly at a rate of 4 °C/h until colorless, block crystals came forth on the matrix. Finally, the melt was cooled to room temperature with the power off. Millimeter-sized $CsZn_2B_3O_7$ crystals (Figure 1) were physically separated from the matrix.

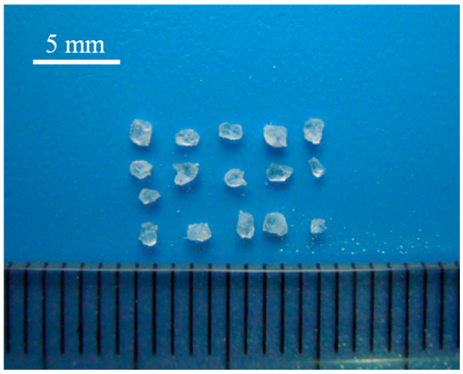

Figure 1. Photograph of $CsZn_2B_3O_7$ crystals.

Elemental Analysis. Elemental analysis of the crystals was performed by using a Jobin Yvon Ultima2 inductively coupled plasma optical emission spectrometer (ICP-OES) with Sepex Certiprep standards. The crystal samples were dissolved in nitric acid at the boiling point for 1 h. The calculated elemental ratio for $CsZn_2B_3O_7$ is Cs/Zn/B = 1.0:2.0:3.2, which is in good agreement with the compositions determined by single-crystal XRD analysis.

Single-Crystal X-ray Diffraction. A colorless $CsZn_2B_3O_7$ crystal of 0.18 × 0.14 × 0.09 mm^3 was selected for single-crystal XRD analysis. The diffraction data were collected with the use of graphite-monochromatized Mo Kα radiation (λ = 0.71073 Å) at 230.01(10) K on an Agilent SuperNova Dual diffractometer with an Atlas detector. The collection of the intensity data, cell refinement, and data reduction were carried out with the program CrysAlisPro.[15] The structure was solved by the direct method with program SHELXS and refined with the least-squares program SHELXL.[16] Final refinement includes anisotropic displacement parameters. The structure was verified using the ADDSYM algorithm from the program PLATON,[17] and no higher symmetries were found. The Flack factor for the compound is close to zero (0.07(4)), which indicates that the absolute structure is correct. Details of crystal parameters, data collection, and structure refinement are summarized in Table 1. In the Supporting Information, Table S1 lists the atomic coordinates and equivalent isotropic displacement parameters, as well as the results of bond valence sum (BVS) calculations.[18] As shown in Supporting Information, Table S1, the BVS calculations give values close to the expected valences for Cs^+, Zn^{2+}, and B^{3+} cations, respectively. The selected bond distances and angles are presented in Supporting Information, Table S2, and the anisotropic displacement parameters are listed in Supporting Information, Table S3.

Thermal Stability. The thermal stability of $CsZn_2B_3O_7$ was investigated by the differential scanning calorimetric (DSC) analysis on a NETZSCH DTA404PC thermal analyzer (the DSC was calibrated with Al_2O_3). About 31.6 mg of $CsZn_2B_3O_7$ was placed in a Al_2O_3 crucible, heated at a rate of 20 °C/min from room temperature to 1050 °C, and then cooled to room temperature at the same rate. The measurement was carried out in an atmosphere of flowing N_2. Thermogravimetric analysis (TGA) of $CsZn_2B_3O_7$ was carried out on a NETZSCH STA

dx.doi.org/10.1021/ic402667m | Inorg. Chem. 2014, 53, 2521−2527

Table 1. Crystal Data and Structure Refinement for $CsZn_2B_3O_7$

formula sum	$CsZn_2B_3O_7$
formula weight (g/mol)	408.08
crystal system	orthorhombic
space group	$Cmc2_1$ (36)
unit cell dimensions (Å)	a = 8.4293(2), b = 19.2550(6), c = 14.5767(4)
V (Å^3)	2365.89(11)
Z	12
μ (mm^{-1})	10.625
F(000)	2232
data/restraints/parameters	1887/1/155
R(int)	0.0318
GOF (F^2)	1.023
flack parameter	0.07(4)
final R indices $[F_o^2 > 2\sigma(F_c^2)]^a$	R_1 = 0.0309, wR_2 = 0.0615
final R indices (all data)^a	R_1 = 0.0362, wR_2 = 0.0581

$^a R1 = \sum||F_o| - |F_c||/\sum|F_o|$; $wR2 = [\sum[w(F_o^2 - F_c^2)^2]/\sum[w(F_o^2)^2]]^{1/2}$ for $F_o^2 > 2\sigma(F_c^2)$.

449C unit. The powders (~20 mg) were placed in a Al_2O_3 crucible that was heated at a rate of 20 °C/min in the range of 25−1050 °C under flowing N_2.

UV−visible−Near-IR Diffuse Reflectance Spectroscopy. The UV−visible−near-IR (UV−vis−NIR) diffuse reflection data were recorded at room temperature using a powder sample with $BaSO_4$ as a standard (100% reflectance) on a PerkinElmer Lamda-900 UV/vis/NIR spectrophotometer. The scanning range is from the wavelength 190 to 1200 nm.

Second-Harmonic Generation Measurements. Powder SHG measurements were carried out by the Kurtz−Perry method.[19] The measurements were performed with a Q-switched Nd:YAG laser at 1064 nm. Polycrystalline $CsZn_2B_3O_7$ was ground and sieved into the following particle size ranges: 30−55, 55−75, 75−125, 125−188, 188−250, and 250−300 μm. The samples were pressed between glass microscope cover slides and secured with tape in 1 mm thick aluminum holders containing an 8-mm diameter hole. The holders were then placed in a light-tight box and irradiated with a laser of wavelength 1064 nm. The intensity of the frequency-doubled output emitted from the samples was collected by a photomultiplier tube. Crystalline KDP was also ground and sieved into the same particle size ranges and used as the references.

3. THEORETICAL METHODS

The first-principles spin-polarized electronic structure calculations were performed using CASTEP, a plane-wave pseudopotential total energy package based on density functional theory (DFT).[20] The gradient-corrected exchange-correlation functionals developed by Perdew, Burke, and Ernzerhof (PBE)[21] were adopted. The interaction between ions and electrons was modeled by optimized norm-conserving pseudopotential in Kleinman−Bylander form,[22] with Cs $5p^66s^1$, Zn $3d^{10}4s^2$, B $2s^22p^1$, and O $2s^22p^4$ treated as valence electrons. Kinetic energy cutoff of 800 eV and Monkhorst−Pack[23] k-point meshes with a density of 2 × 2 × 1 points in the Brillouin zone were chosen. Our convergence tests show that the choice of above computational parameters is sufficiently accurate for this Study.

It is well-known that the band gap calculated by DFT is smaller than the experimental data due to the discontinuity of correlation function, so a scissors operator[24] was used to shift all the conduction band (CB) upward to agree with the measured data. On the basis of the calculated electronic band structure, we can obtain the imaginary part of the dielectric function from the electronic transition between valence band (VB) and CB.[25] Consequently, the real part of the dielectric function, that is, the refractive indices, can be determined by Kramers−Kronics transform. Meanwhile, the SHG coefficients can be obtained by the formula developed by our group.[26] To analyze the contribution of an ion (or ionic group) to the nth order susceptibility $\chi^{(n)}$, a real-space atom-cutting technique was adopted.[26] Within this method the contribution of ion A to the nth-order susceptibility (denoted as $\chi^{(n)}(A)$) can be obtained by cutting all ions except A from the original wave functions $\chi^{(n)}(A) = \chi^{(n)}$ (all ions except A are cut).

4. RESULTS AND DISCUSSION

Thermal Behavior. As shown in Figure 2, the DSC data show two sharp endothermic peaks around 954 and 1009 °C,

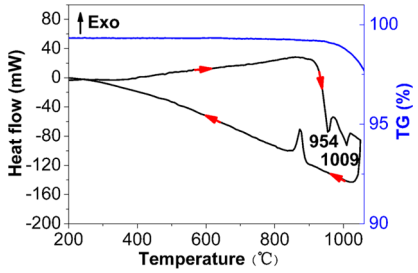

Figure 2. DSC and TGA curves of $CsZn_2B_3O_7$.

respectively, in the heating curve, and the TGA data do not show weight loss until ~950 °C. These results indicate that $CsZn_2B_3O_7$ is an incongruently melting compound. To further verify the thermal behavior, two $CsZn_2B_3O_7$ powder samples were sintered at 980 and 1020 °C, respectively, for 1 d. While they were cooled to room temperature with the power off, needle and plate-like crystals were obtained, respectively. As revealed by single-crystal XRD analysis, the aforementioned two endothermic peaks can be ascribed to the decomposition of $CsZn_2B_3O_7$ into $CsZn_4(BO_3)_3$[27] and the further decomposition into $Zn_3(BO_3)_2$,[28] respectively. This confirmed the incongruent-melting behavior of $CsZn_2B_3O_7$. Therefore, large crystals of $CsZn_2B_3O_7$ should be grown using flux method below the decomposition temperature.

Crystal Structure. $CsZn_2B_3O_7$ crystallizes in the orthorhombic crystal system with a polar NCS space group of $Cmc2_1$. The crystal structure is composed of two-dimensional (2D) $[Zn_2BO_5]_\infty$ layers that are bridged by planar $[B_3O_6]^{3-}$ groups along the b axis to construct a three-dimensional (3D) framework with one-dimensional (1D) channels running along the a and c axes (Figure 3a,b). Cs^+ cations reside in the 1D channels to maintain the charge balance. In the structure of $CsZn_2B_3O_7$, there are six crystallographically independent boron atoms, which are all three-coordinated to form planar $[BO_3]^{3-}$ or $[B_3O_6]^{3-}$ groups. The B−O distances and O−B−O angles are in the ranges of 1.294(17)−1.422(19) Å and 116.3(12)−123.7(13)°, respectively. Zn atoms occupy three independent sites and are four-coordinated to form irregular ZnO_4 tetrahedra. The Zn−O distances and O−Zn−O

dx.doi.org/10.1021/ic402667m | Inorg. Chem. 2014, 53, 2521−2527

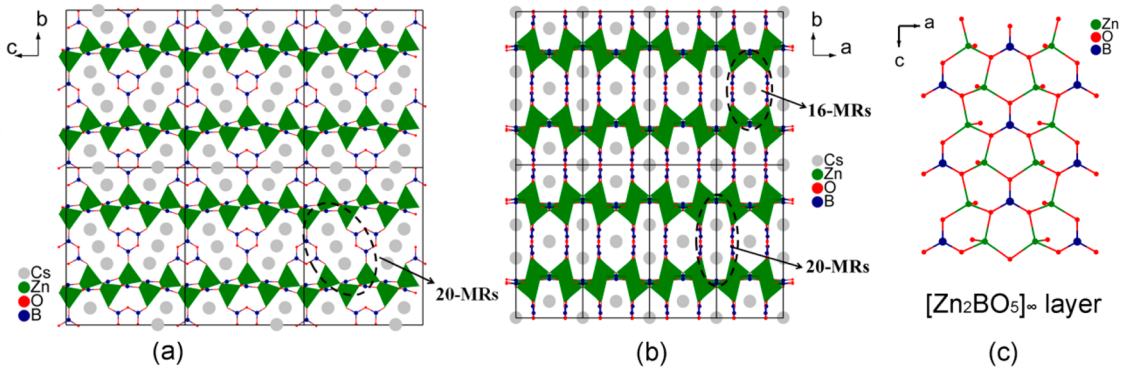

Figure 3. (a) View of the $CsZn_2B_3O_7$ structure along the *a* axis. (b) View of the $CsZn_2B_3O_7$ structure along the *c* axis. (c) View of the $[Zn_2BO_5]_\infty$ layer along the *b* axis. The green polyhedra represent ZnO_4 tetrahedra; the 1D channels along the *a* axis are composed of 20-membered rings (20-MRs), while along the *c* axis they are based on 16-MRs and 20-MRs.

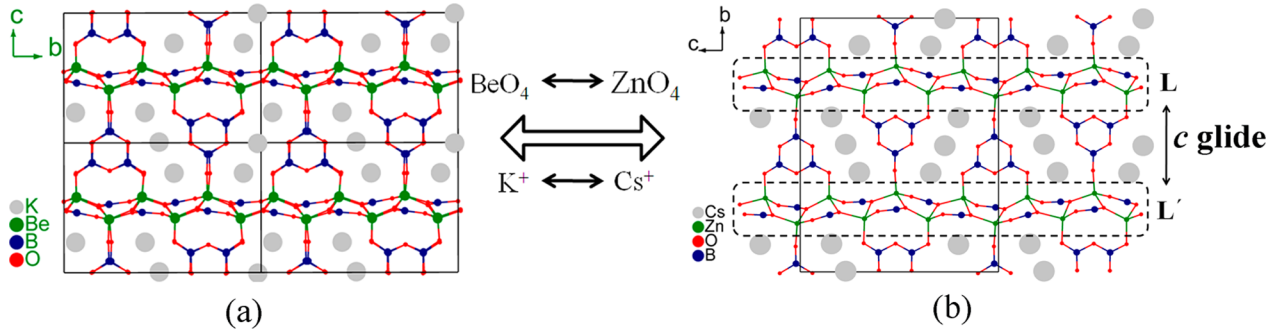

Figure 4. View along the *a* axis for (a) the γ-$KBe_2B_3O_7$ structure and (b) the $CsZn_2B_3O_7$ structure.

angles are also normal (see Table S2 in the Supporting Information). Each ZnO_4 tetrahedron is linked to three neighboring $[BO_3]^{3-}$ groups by sharing basal oxygen atoms to form a 2D [3, 3] $[Zn_2BO_5]_\infty$ layer (Figure 3c) in the *ab* plane. The rest apical oxygen atoms of ZnO_4 tetrahedra alternately dangle up and down the 2D $[Zn_2BO_5]_\infty$ layer to link the $[B_3O_6]^{3-}$ groups, which serve as bridges of the adjacent $[Zn_2BO_5]_\infty$ layers. Within a single $[Zn_2BO_5]_\infty$ layer, the [3, 3] connection of ZnO_4 tetrahedra and $[BO_3]^{3-}$ groups makes all $[BO_3]^{3-}$ groups in an approximately coplanar and aligned arrangement (Figure 3c). In each $CsZn_2B_3O_7$ unit cell, there are two $[Zn_2BO_5]_\infty$ layers L and L′, which are related to a *c* glide plane from each other (Figure 4b). With respect to the $[B_3O_6]^{3-}$ groups, they are parallel to each other along the *b* axis, but one-half of them are arranged in a manner opposite to the other half (Figure 4b).

The crystal structure of $CsZn_2B_3O_7$ is closely related to that of γ-$KBe_2B_3O_7$,[14d] which consists of 2D $[Be_2BO_5]_\infty$ layers that are also bridged through $[B_3O_6]^{3-}$ planar groups (Figure 4a). The $[Zn_2BO_5]_\infty$ layers can be regarded as a variant of $[Be_2BO_5]_\infty$ layers by substituting BeO_4 tetrahedra for ZnO_4 tetrahedra (Figure 4). Within $[Zn_2BO_5]_\infty$ and $[Be_2BO_5]_\infty$ layers, the tetrahedra and BO_3 triangles have the same [3, 3] connection mode, which leads to the coplanar and aligned arrangement of BO_3 triangles (Supporting Information, Figure S2). In the structures of both $CsZn_2B_3O_7$ and γ-$KBe_2B_3O_7$, there are three types of 1D channels, which are based on 16-membered rings (16-MRs) and two types of 20-MRs (see Supporting Information, Figure S3). Since the Zn−O distances are longer than Be−O distances, in $CsZn_2B_3O_7$ the multi-MRs, which are composed of ZnO_4 tetrahedra and BO_3 triangles, are of larger sizes in comparison with the corresponding 1D channels in γ-$KBe_2B_3O_7$ (see Supporting Information, Figure S3). As a result, Cs^+ cations are desired to fill the Zn−B−O 1D channels, following the ionic radius trend $Cs^+ > K^+$.

Easiness for the Growth of Bulk Crystals. Since the structure of $CsZn_2B_3O_7$ features $[Zn_2BO_5]_\infty$ layers bridged by covalent $[B_3O_6]^{3-}$ groups, it is necessary to evaluate the interlayer interactions. Take KBBF as an example, the adjacent $[Be_2BO_3F_2]_\infty$ layers are weakly connected by the K^+−F^- ionic bonds, which results in a great difficulty in the growth of thick crystals, namely, layering tendency. In the case of $CsZn_2B_3O_7$, the $[B_3O_6]^{3-}$ groups afford a very strong interlayer connection through the covalent B−O bonds, indicating that the interlayer connection of $CsZn_2B_3O_7$ is greatly reinforced as compared with that of KBBF. In our preliminary attempts for crystal growth, the obtained crystals are of block shape without layering tendency (Figure 1), which experimentally confirms the aforementioned analysis from the point of view of microscopic crystal structure. This result indicates that thick $CsZn_2B_3O_7$ crystals can be obtained.

Linear and Nonlinear Optical Properties. As shown in Figure 5, $CsZn_2B_3O_7$ is transparent down to the UV spectral region, with a short absorption edge at 218 nm (corresponding to a band gap of 5.69 eV), which suggests that it may find applications in UV region. Because $CsZn_2B_3O_7$ crystallizes in a NCS space group, it is expected to possess NLO properties. The curves of SHG intensity as a function of particle size are shown in Figure 6. The SHG intensities increase with increasing particle sizes before they become constant in the particle size range of 188−300 μm, which is consistent with type I phase-matching behavior on the basis of the rule proposed by Kurtz and Perry.[19] At the same particle sizes of 250−300 μm, $CsZn_2B_3O_7$ exhibits a SHG efficiency of about

dx.doi.org/10.1021/ic402667m | Inorg. Chem. 2014, 53, 2521−2527

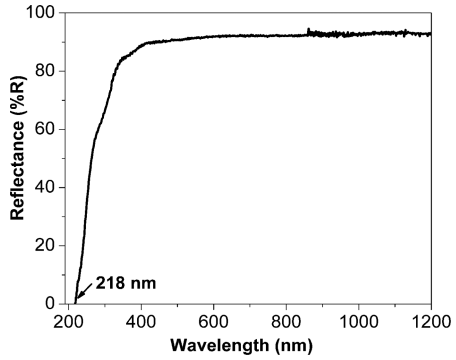

Figure 5. UV−vis−NIR diffuse reflectance spectrum of $CsZn_2B_3O_7$.

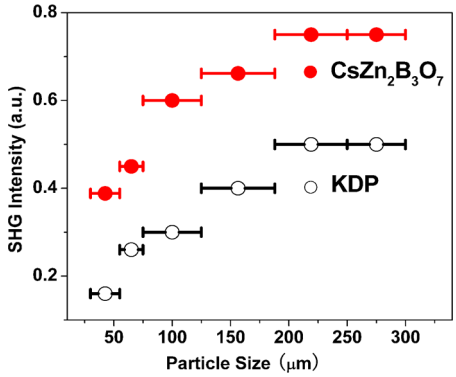

Figure 6. SHG intensity as a function of particle size for $CsZn_2B_3O_7$. KDP serves as the reference.

1.5 × KDP, which is comparable to that of KBBF (1.21 × KDP).[13] Considering the UV transparency, phase-matchability, and a relatively large SHG response, $CsZn_2B_3O_7$ may have prospects in UV region as a NLO material. It is notable that the SHG efficiency of $CsZn_2B_3O_7$ is about 2-fold that of γ-$KBe_2B_3O_7$ (0.68 × KDP)[14d] despite they afford the similarly arranged NLO-active units ($[BO_3]^{3-}$ groups) and the same interlayer bridges ($[B_3O_6]^{3-}$ groups).

Origin of the SHG Enhancement. To reveal why $CsZn_2B_3O_7$ exhibits an enhanced SHG efficiency in comparison with γ-$KBe_2B_3O_7$, the first-principles calculations were performed. The electronic band structures of $CsZn_2B_3O_7$, along the lines of high symmetry points in the Brillouin zone, are shown in Figure 7a, which shows that $CsZn_2B_3O_7$ is an indirect gap crystal and that the direct gap at G is 0.02 eV larger than the indirect band gap. The partial density of state (PDOS) projected on the constitutional atoms of $CsZn_2B_3O_7$ is shown in Figure 7b. Clearly, the deep part of VB lower than −15 eV is mainly composed of Cs 5s and O 2s orbitals. The upper part of the VB (−10 to 0 eV) consists of Cs 5p (localized at about −7 eV), Zn 3d, and B and O 2p orbitals, and the strong hybridization between oxygen and the neighbor atoms is exhibited. However, the VB maximum is exclusively occupied by O 2p orbitals. The bottom of the CB is contributed from the orbitals of all atoms in $CsZn_2B_3O_7$, but the electronic states on Zn are located at the CB minimum and thus determine the bandgap. Since the optical effects of a crystal are mainly determined by the optical transition between the electronic states close to the bandgap,[29] it is anticipated that they are dominantly contributed from the groups constructed by O, B, and Zn, while the contribution from the orbitals of the Cs^+ cations is negligibly small.

On the basis of the electronic band structures, the linear and nonlinear optical properties in $CsZn_2B_3O_7$ were calculated (see Table 2). Because $CsZn_2B_3O_7$ belongs to the orthorhombic crystal system with a space group of $Cmc2_1$, it has three nonzero independent SHG coefficients, namely, d_{31}, d_{32}, and d_{33}. The calculated results are d_{31} = 0.404 pm/V, d_{32} = −0.053 pm/V, and d_{33} = −0.165 pm/V, which are in agreement with

Table 2. Calculated Linear and Nonlinear Optical Properties for $CsZn_2B_3O_7$, as well as the Real-Space Atom-Cutting Analysis[a]

	total	$[ZnO_4]^{6-}$	$[BO_3]^{3-}$	$[B_3O_6]^{3-}$	Cs^+
n_x	1.542	1.263	1.216	1.240	1.186
n_y	1.565	1.228	1.177	1.303	1.183
n_z	1.598	1.267	1.221	1.302	1.191
Δn	0.056	0.039	0.044	0.062	0.008
d_{31}	0.404	0.203	0.126	0.049	0.026
d_{32}	−0.053	−0.019	−0.015	−0.016	0.008
d_{33}	−0.165	−0.020	−0.057	−0.040	−0.048

[a]The birefringence Δn is obtained by the difference between the largest and smallest refractive indices.

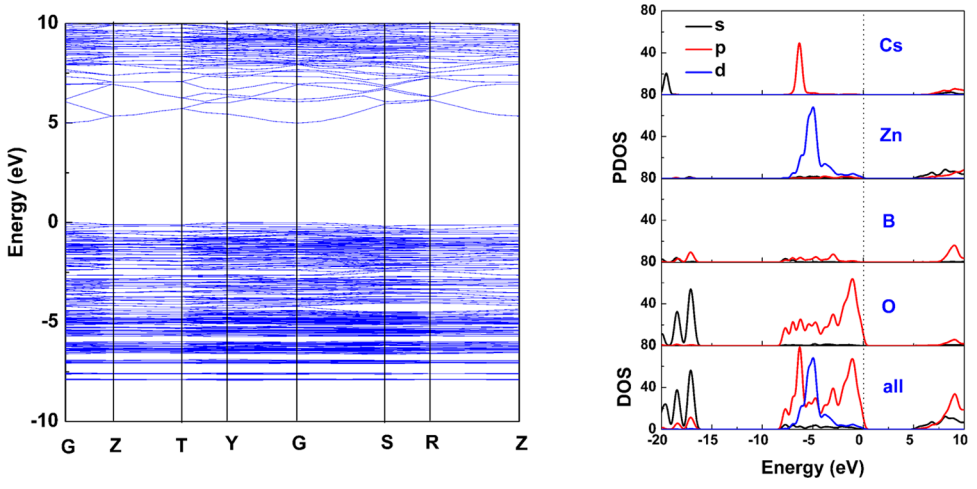

Figure 7. Electronic properties in $CsZn_2B_3O_7$. (a) Band structure. (b) DOS and PDOS.

dx.doi.org/10.1021/ic402667m | Inorg. Chem. 2014, 53, 2521−2527

the powder SHG measurements and verify the validity of our first-principles method on the studied crystal. Moreover, we predict that the optical birefringence in $CsZn_2B_3O_7$ is Δn = 0.056 (at an incident wavelength of 1064 nm), which is close to that of KBBF (Δn = 0.070).[13] Such a large birefringence is consistent with the phase-matching behavior observed in the SHG experiments.

To further analyze the contribution of the constituent groups (or ions) in $CsZn_2B_3O_7$ to the linear and nonlinear optical coefficients, the real-space atom-cutting analysis was performed (see Table 2). It is exhibited that the respective contributions to the dominant SHG coefficient d_{31} are 0.203 pm/V for $[ZnO_4]^{6-}$ (50% of d_{31}), 0.126 pm/V for $[BO_3]^{3-}$ (33% of d_{31}), 0.049 pm/V for $[B_3O_6]^{3-}$ (13% of d_{31}), and 0.026 pm/V for Cs^+ (5% of d_{31}). Clearly, the ZnO_4 tetrahedra combined with the anionic $[BO_3]^{3-}$ groups make the dominant contribution to d_{31}, while the contribution of Cs^+ cations and $[B_3O_6]^{3-}$ groups is negligibly small. The situation in which the $[B_3O_6]^{3-}$ groups have a very small contribution to the NLO effects is in contrast to the case in BBO, where the $[B_3O_6]^{3-}$ groups result in very large SHG coefficients. It is due to the antiparallel arrangement of the $[B_3O_6]^{3-}$ groups (in the crystal structure of $CsZn_2B_3O_7$), which leads to a cancellation of their microscopic second-order susceptibilities. However, because all $[B_3O_6]^{3-}$ groups are nearly parallel to the *bc* plane, their contribution to the linear optical anisotropy, that is, the birefringence, is evidently dominant and much larger than that of the other groups or ions.

It should be emphasized that the contribution of the $[ZnO_4]^{6-}$ groups to the SHG effect is significantly larger than that from the aligned $[BO_3]^{3-}$ groups in $CsZn_2B_3O_7$. For comparison, in the case of γ-$KBe_2B_3O_7$, the largest calculated SHG coefficient is d_{22} = 0.22 pm/V, and our real-space atom-cutting analysis reveals that the corresponding SHG contribution for $[BO_3]^{3-}$ is 0.19 pm/V, whereas the contributions of $[BeO_4]^{6-}$, $[B_3O_6]^{3-}$, and K^+ are negligibly small. This result clearly demonstrates that $[BO_3]^{3-}$ groups make the dominant contribution to the SHG effect of γ-$KBe_2B_3O_7$, consistent with the conclusion obtained from anionic group theory.[30] Thus, although $CsZn_2B_3O_7$ and γ-$KBe_2B_3O_7$ have similar 2D layers bridged through the same interlayer connectors, their SHG mechanisms are quite different, which lead to a 2-fold contrast with respect to the SHG efficiency. Namely, it is the ZnO_4 tetrahedra that make $CsZn_2B_3O_7$ exhibiting almost the double SHG effects as compared with γ-$KBe_2B_3O_7$. It was reported that the ZnO_4 tetrahedra may be NLO-active in the potential IR NLO materials (e.g., $ZnTeMoO_6$,[31] UV edge ~350 nm), but our studies present in this Work distinguish this type of microscopic group as UV-transparent NLO-active units down to the wavelength of about 200 nm.

5. CONCLUSION

A new noncentrosymmetric borate $CsZn_2B_3O_7$ has been synthesized, and the crystals have been obtained. The crystal structure is composed of $[Zn_2BO_5]_\infty$ 2D layers that are further bridged by $[B_3O_6]^{3-}$ anionic groups to form a 3D framework with 1D channels occupied by Cs^+ cations along the *a* and *c* axes. Owing to the strong interlayer interactions, no layering tendency was observed in $CsZn_2B_3O_7$ crystals, indicating that thick crystals can be obtained. $CsZn_2B_3O_7$ is transparent down to 218 nm in the UV region and is phase-matchable with a powder SHG efficiency of 1.5 × KDP at 1064 nm. Therefore, $CsZn_2B_3O_7$ has prospects as a UV NLO material. Moreover, the SHG efficiency of $CsZn_2B_3O_7$ is about 2-fold that of the structurally analogous γ-$KBe_2B_3O_7$. First-principles calculations and atom-cutting analysis reveal that the ZnO_4 tedrahedra dominate the SHG enhancement, which distinguishes ZnO_4 tedrahedra as a new type of UV-transparent NLO-active units. We believe that a combination of ZnO_4 tetrahedra and π-orbital systems will lead to more UV NLO materials.

■ ASSOCIATED CONTENT

Ⓢ Supporting Information

The multi-MRs in γ-$KBe_2B_3O_7$ and $CsZn_2B_3O_7$, crystallographic parameters, crystal data in CIF format are included here, as are powder XRD patterns for $CsZn_2B_3O_7$. This material is available free of charge via the Internet at http://pubs.acs.org.

■ AUTHOR INFORMATION

Corresponding Author

*E-mail: zslin@mail.ipc.ac.cn (Z.L.), jhluo@fjirsm.ac.cn (J.L.).

Notes

The authors declare no competing financial interest.

■ ACKNOWLEDGMENTS

This work was financially supported by the National Natural Science Foundation of China (21222102, 21373220, 51102231, 21171166, 11174297, and 91022036), the One Hundred Talent Program of the Chinese Academy of Sciences, the National Basic Research Project of China (2010CB630701, 2010CB933501, 2011CB922204, 2011CB935904), the Key Project of Fujian Province (2012H0045), and the opening fund of Key Laboratory of Functional Crystals and Laser Technology, TIPC, CAS (FCLT 201306).

■ REFERENCES

(1) (a) Becker, P. *Adv. Mater.* **1998**, *10*, 979. (b) Sasaki, T.; Mori, Y.; Yoshimura, M.; Yap, Y. K.; Kamimura, T. *Mat. Sci. Eng., R* **2000**, *30*, 1.

(2) (a) Halasyamani, P. S.; Poeppelmeier, K. R. *Chem. Mater.* **1998**, *10*, 2753. (b) Donakowski, M. D.; Gautier, R.; Yeon, J. H.; Moore, D. T.; Nino, J. C.; Halasyamani, P. S.; Poeppelmeier, K. R. *J. Am. Chem. Soc.* **2012**, *134*, 7679.

(3) Yeon, J.; Kim, S. H.; Halasyamani, P. S. *Inorg. Chem.* **2010**, *49*, 6986.

(4) (a) Kim, S. H.; Yeon, J.; Halasyamani, P. S. *Chem. Mater.* **2009**, *21*, 5335. (b) Nguyen, S. D.; Yeon, J.; Kim, S. H.; Halasyamani, P. S. *J. Am. Chem. Soc.* **2011**, *133*, 12422. (c) Lee, D. W.; Kim, S. B.; Ok, K. M. *Dalton Trans.* **2012**, *41*, 8348. (d) Yeon, J.; Kim, S. H.; Hayward, M. A.; Halasyamani, P. S. *Inorg. Chem.* **2011**, *50*, 8663.

(5) (a) Chung, I.; Kanatzidis, M. G. *Chem. Mater.* **2013**, Article ASAP, DOI: 10.1021/cm401737s. (b) Choi, K. S.; Kanatzidis, M. G. *Chem. Mater.* **1999**, *11*, 2613.

(6) (a) Barbier, J.; Penin, N.; Cranswick, L. M. *Chem. Mater.* **2005**, *17*, 3130. (b) McMillen, C. D.; Stritzinger, J. T.; Kolis, J. W. *Inorg. Chem.* **2012**, *51*, 3953. (c) Wang, L.; Pan, S.; Chang, L.; Hu, J.; Yu, H. *Inorg. Chem.* **2012**, *51*, 1852. (d) Zhang, W. L.; Cheng, W. D.; Zhang, H.; Geng, L.; Lin, C. S.; He, Z. Z. *J. Am. Chem. Soc.* **2010**, *132*, 1508. (e) Zhao, S. G.; Zhang, G. C.; Yao, J. Y.; Wu, Y. C. *CrystEngComm* **2012**, *14*, 5209. (f) Gao, J.; Li, S. *Inorg. Chem.* **2012**, *51*, 420. (g) Heyward, C.; McMillen, C.; Kolis, J. *Inorg. Chem.* **2012**, *51*, 3956. (h) Wu, H.; Pan, S.; Poeppelmeier, K. R.; Li, H.; Jia, D.; Chen, Z.; Fan, X.; Yang, Y.; Rondinelli, J. M.; Luo, H. *J. Am. Chem. Soc.* **2011**, *133*, 7786. (i) Wu, L.; Chen, X. L.; Xu, Y. P.; Sun, Y. P. *Inorg. Chem.* **2006**, *45*, 3042. (j) Wu, H. P.; Yu, H. W.; Yang, Z. H.; Hou, X. L.; Su, X.; Pan, S. L.; Poeppelmeier, K. R.; Rondinelli, J. M. *J. Am. Chem. Soc.* **2013**, *135*, 4215.

(7) Kang, L.; Ramo, D. M.; Lin, Z. S.; Bristowe, P. D.; Qin, J. G.; Chen, C. T. *J. Mater. Chem. C* **2013**, Article ASAP, DOI:10.1039/C3TC31283F.
(8) (a) Cao, Z.; Yue, Y.; Yao, J.; Lin, Z.; He, R.; Hu, Z. *Inorg. Chem.* **2011**, *50*, 12818. (b) Huang, Y. Z.; Wu, L. M.; Wu, X. T.; Li, L. H.; Chen, L.; Zhang, Y. F. *J. Am. Chem. Soc.* **2010**, *132*, 12788. (c) Sun, C. F.; Hu, C. L.; Xu, X.; Ling, J. B.; Hu, T.; Kong, F.; Long, X. F.; Mao, J. G. *J. Am. Chem. Soc.* **2009**, *131*, 9486. (d) Zhao, S. G.; Jiang, X. X.; He, R.; Zhang, S. Q.; Sun, Z. H.; Luo, J. H.; Lin, Z. S.; Hong, M. C. *J. Mater. Chem. C* **2013**, *1*, 2906. (e) Ra, H. S.; Ok, K. M.; Halasyamani, P. S. *J. Am. Chem. Soc.* **2003**, *125*, 7764. (f) Yu, Q.; Gao, Z.; Zhang, S.; Zhang, W.; Wang, S.; Tao, X. *J. Appl. Phys.* **2012**, *111*, 013506. (g) Zhang, W. G.; Tao, X. T.; Zhang, C. Q.; Gao, Z. L.; Zhang, Y. Z.; Yu, W. T.; Cheng, X. F.; Liu, X. S.; Jiang, M. H. *Cryst. Growth Des.* **2008**, *8*, 304. (h) Suffren, Y.; Gautier-Luneau, I. *Eur. J. Inorg. Chem.* **2012**, 4264. (i) Bera, T. K.; Jang, J. I.; Ketterson, J. B.; Kanatzidis, M. G. *J. Am. Chem. Soc.* **2009**, *131*, 75.
(9) Chen, C. T.; Wu, Y. C.; Jiang, A. D.; Wu, B. C.; You, G. M.; Li, R. K.; Lin, S. J. *J. Opt. Soc. Am. B* **1989**, *6*, 616.
(10) Chen, C. T.; Wu, B. C.; Jiang, A. D.; You, G. M. *Sci. Sin., Ser. B* **1985**, *28*, 235.
(11) (a) Mori, Y.; Kuroda, I.; Nakajima, S.; Sasaki, T.; Nakai, S. *Appl. Phys. Let.* **1995**, *67*, 1818. (b) Tu, J. M.; Keszler, D. A. *Mater. Res. Bull.* **1995**, *30*, 209.
(12) (a) Xia, Y. N.; Chen, C. T.; Tang, D. Y.; Wu, B. C. *Adv. Mater.* **1995**, *7*, 79. (b) Cyranoski, D. *Nature* **2009**, *457*, 953.
(13) Chen, C. T.; Wang, G. L.; Wang, X. Y.; Xu, Z. Y. *Appl. Phys. B: Lasers Opt.* **2009**, *97*, 9.
(14) (a) Chen, C. T.; Wang, Y. B.; Wu, B. C.; Wu, K. C.; Zeng, W. L.; Yu, L. H. *Nature* **1995**, *373*, 322. (b) Wang, S. C.; Ye, N. *J. Am. Chem. Soc.* **2011**, *133*, 11458. (c) Huang, H. W.; Yao, J. Y.; Lin, Z.; Wang, X. Y.; He, R.; Yao, W. J.; Zhai, N. X.; Chen, C. T. *Chem. Mater.* **2011**, *23*, 5457. (d) Wang, S. C.; Ye, N.; Li, W.; Zhao, D. *J. Am. Chem. Soc.* **2010**, *132*, 8779. (e) Huang, H.; Yao, J.; Lin, Z.; Wang, X.; He, R.; Yao, W.; Zhai, N.; Chen, C. *Angew. Chem., Int. Ed. Engl.* **2011**, *50*, 9141.
(15) *CrysAlisPro, Version 1.171.36.28;* Agilent Technologies: Santa Clara, CA, 2013.
(16) Sheldrick, G. M. *Acta Crystallogr. A* **2008**, *64*, 112.
(17) Spek, A. L. *J. Appl. Crystallogr.* **2003**, *36*, 7.
(18) Brown, I. D.; Altermatt, D. *Acta Crystallogr. B* **1985**, *41*, 244.
(19) Kurtz, S. K.; Perry, T. T. *J. Appl. Phys.* **1968**, *39*, 3798.
(20) Kohn, W.; Sham, L. J. *Phys. Rev.* **1965**, *140*, A1133.
(21) Perdew, J. P.; Burke, K.; Ernzerhof, M. *Phys. Rev. Lett.* **1996**, *77*, 3865.
(22) Kleinman, L.; Bylander, D. M. *Phys. Rev. Lett.* **1982**, *48*, 1425.
(23) Monkhors, H. J.; Pack, J. D. *Phys. Rev. B* **1976**, *13*, 5188.
(24) Godby, R. W.; Schluter, M.; Sham, L. J. *Phys. Rev. B* **1988**, *37*, 10159.
(25) Masia, M.; Probst, M.; Rey, R. *J. Chem. Phys.* **2004**, *121*, 7362.
(26) (a) Lin, J.; Lee, M. H.; Liu, Z. P.; Chen, C. T.; Pickard, C. J. *Phys. Rev. B* **1999**, *60*, 13380. (b) Lin, Z. S.; Lin, J.; Wang, Z. Z.; Wu, Y. C.; Ye, N.; Chen, C. T.; Li, R. K. *J. Phys.: Condens. Matter* **2001**, *13*, R369.
(27) Smith, R. W.; Luce, J. L.; Keszler, D. A. *Inorg. Chem.* **1992**, *31*, 4679.
(28) Chen, D. G.; Cheng, W. D.; Wu, D. S.; Zhang, H.; Zhang, Y. C.; Gong, Y. J.; Kan, Z. G. *Solid State Sci.* **2005**, *7*, 179.
(29) Lee, M.-H.; Y, C.-H.; Jan, J.-H. *Phys. Rev. B* **2004**, *70*, 235110.
(30) Chen, C. *Sci. Sin.* **1979**, *22*, 756.
(31) Zhao, S. G.; Luo, J. H.; Zhou, P.; Zhang, S. Q.; Sun, Z. H.; Hong, M. C. *RSC Adv.* **2013**, *3*, 14000.